IOPscience iopscience.iop.org

Home Search Collections Journals About Contact us My IOPscience

Observation of nonlinear couplings between coexisting kinetic geodesic acoustic modes in the edge plasmas of the HT-7 tokamak

This content has been downloaded from IOPscience. Please scroll down to see the full text.

2013 Nucl. Fusion 53 113008

(http://iopscience.iop.org/0029-5515/53/11/113008)

View the table of contents for this issue, or go to the journal homepage for more

Download details:

IP Address: 202.127.206.120
This content was downloaded on 21/07/2014 at 07:30

Please note that terms and conditions apply.

IOP Publishing and International Atomic Energy Agency Nuclear Fusion

Nucl. Fusion **53** (2013) 113008 (9pp) doi:10.1088/0029-5515/53/11/113008

Observation of nonlinear couplings between coexisting kinetic geodesic acoustic modes in the edge plasmas of the HT-7 tokamak

D.F. Kong[1], A.D. Liu[1], T. Lan[1], Z.Y. Qiu[2], H.L. Zhao[1], H.G. Sheng[1], C.X. Yu[1], L. Chen[2,3], G.S. Xu[4], W. Zhang[4], B.N. Wan[4], R. Chen[4], W.X. Ding[1,5], X. Sun[1], J.L. Xie[1], H. Li[1] and W.D. Liu[1]

[1] CAS Key Laboratory of Geospace Environment, Department of Modern Physics, University of Science and Technology of China, Hefei 230026, People's Republic of China
[2] Institute for Fusion Theory and Simulation, Zhejiang University, Hangzhou 310027, People's Republic of China
[3] Department of Physics and Astronomy, University of California, Irvine, CA 92697-4575, USA
[4] Institute of Plasma Physics, Chinese Academy of Sciences, Hefei 230031, People's Republic of China
[5] Department of Physics and Astronomy, University of California at Los Angeles, Los Angeles, CA 90095, USA

E-mail: lad@ustc.edu.cn

Received 8 May 2013, accepted for publication 20 August 2013
Published 16 September 2013
Online at stacks.iop.org/NF/53/113008

Abstract
Coexisting multi-geodesic acoustic modes (GAMs), especially coexisting dual GAMs, are observed and studied through Langmuir probe arrays at the edge plasmas of the HT-7 tokamak with lithium-coated walls. The dual GAMs are named a low-frequency GAM (LFGAM) and a high-frequency GAM (HFGAM), and it is found that within the measuring range, the HFGAM propagates outwards while the LFGAM propagates both inwards and outwards with their central frequencies nearly unchanged, and both modes have maximum amplitudes at positions with radial wavenumbers close to zero; meanwhile, the two positions happen to be where the continuum GAM frequency is closest to the central frequencies of the LFGAM and the HFGAM. These characteristics are consistent with those of a kinetic GAM converted from a continuum GAM. The nonlinear couplings between the LFGAM and the HFGAM are also analysed. In this study, we observed not only the interaction between the LFGAM and the HFGAM, but also the self-coupling of the GAM with the beat frequency between them, as well as the coupling between the LFGAM and an unknown mode at ~50 kHz. These nonlinear interactions may play important roles during the saturation process of GAMs. Additionally, amplitude correlation analyses of multi-GAMs indicate that second harmonic GAMs are probably generated from the self-interaction of fundamental GAMs.

(Some figures may appear in colour only in the online journal)

1. Introduction

Geodesic acoustic modes (GAMs) [1], which are the high-frequency branch of zonal flows, are azimuthally symmetric modes unique to toroidal plasmas. GAMs are characterized by potential fluctuations with $m = n = 0$ and density fluctuations with $m/n = 1/0$ (m/n is the poloidal/toroidal mode number). Recently, GAMs have received considerable attention in magnetic fusion plasma research due to the important role in controlling the transport level of the plasmas through nonlinear interaction with drift-wave turbulence [2, 3], which is further enhanced by the observation of a competition between the turbulence level and GAM flow shearing in the limit-cycle phase on ASDEX-U [4]. The dispersion relation of GAMs was first derived via fluid theory and the linear dependence of the GAM frequency on the ion acoustic velocity C_s, i.e. the so-called continuum GAM, has already been observed in various fusion devices [5–9].

 © 2013 IAEA, Vienna Printed in the UK & the USA

However, the existence of GAM eigenmode was also reported, especially at the edge plasmas. In JFT-2M, it was found that the GAM frequencies remained constant along the radial direction at several centimetres just inside the last closed flux surface (LCFS) [10] and similar phenomena were also observed in the HL-2A and HT-7 tokamaks [11, 12]; multi-GAMs or splitting of GAM spectra at edge plasmas have also been reported on the T-10 and ASDEX-U tokamaks [13, 14]; in DIII-D, continuum GAM and eigenmode-type GAM have both been observed through Doppler backscattering systems under different discharge conditions [15]. Theoretical and simulated results suggested that kinetic effects should be considered to access these phenomena conflicting with the dispersion relation deduced from fluid theory [16–18]. The concept of kinetic GAM (KGAM) was first proposed by Zonca [19], indicating that on considering the finite ion Larmor radius effects, the existence of a singular layer would cause a continuum GAM to transform to a KGAM, whereas comparisons between theoretical and experimental results of KGAMs are scarce. Another important issue of GAM is the nonlinear interaction of GAMs, especially the self-coupling of GAMs, which was first reported in the JFT-2M tokamak [20]. Theoretical and simulated analyses suggested that the nonlinear interactions probably offer an important saturation mechanism for GAMs and the generation of the second harmonic is strongly influenced by the parallel nonlinearity, while further experiments are needed to draw further conclusions [21, 22].

In this work, two coexisting GAMs, sometimes coexisting multi-GAMs, are observed through Langmuir probe arrays in edge plasmas with a low collisionality due to the lithium-coated walls on the HT-7 tokamak. The radial distributions of central frequency, amplitude and radial wavenumber of these GAMs all suggest that they are KGAMs converted from continuum GAMs. Moreover, both cross-coupling and self-coupling between these GAMs are shown, implying that the nonlinear interaction is strongly dependent on the generated position of GAMs. And an amplitude correlation analysis is used to estimate the spectral energy flow between the fundamental GAM and the second harmonic GAM. The paper is organized as follows. The experimental setup is introduced in section 2. Results and discussion are presented in section 3. A summary is given in section 4.

2. Experimental arrangement

HT-7 is a limiter tokamak with $R = 1.22\,\mathrm{m}$, $a = 0.27\,\mathrm{m}$ and a circular poloidal cross-section. Experiments are carried out in an ohmically heated deuterium plasma with the limiter configuration under the following conditions: plasma current $I_\mathrm{p} = 80$–$120\,\mathrm{kA}$, toroidal magnetic field $B_\mathrm{t} = 1.8\,\mathrm{T}$, central-chord-averaged electron density $n_\mathrm{e} = 1.5 \times 10^{19}\,\mathrm{m}^{-3}$ and safety factor at the limiter position $q_a = 4.5$–6.7. Measurements are carried out by two radially movable probe systems marked A and B, and the arrangement is shown in figure 1. Both probe systems are inserted from the top ports of the tokamak. Probe array A is a standard four-tip probe, which is reciprocating and is used for measuring the electron temperature as well as the density and floating potential. Probe array B has seven graphite tips, which are grouped into two steps with 5 mm radial separation. The two tips on the bottom step are Mach probes and on the top step are five tips for measurements of the floating potential and its fluctuations. This arrangement of two probe systems allows simultaneous measurement of floating potential fluctuations ($\tilde{\phi}_\mathrm{f}$) in the toroidal direction with large toroidal separations (256 cm). Our previous experiments in HT-7 [12] and HL-2A [23–25] and experiments in other devices [26, 27] all prove that such an arrangement is effective in measurements of the spatial and temporal structure of zonal flows. Based on the good repeatability of the discharge on HT-7, we could move both the probe systems shot by shot along the radial direction in steps of 0.25 or 0.5 cm till 2 cm inside the LCFS; then the distribution of the amplitude, central frequency as well as the radial wavenumber of GAMs could be estimated, which will be shown in the following.

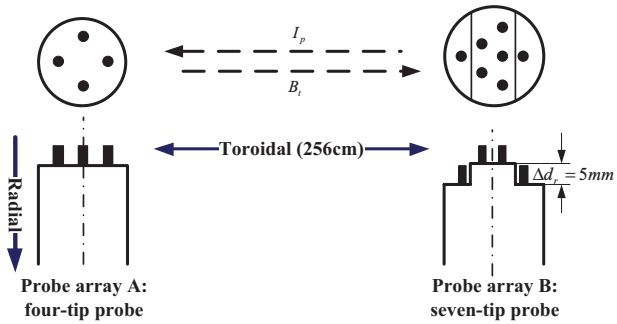

Figure 1. The arrangement of experiments and the structures of probe arrays.

3. Experimental results

3.1. Observation of two coexisting GAMs

Typical results of long-distance correlations of floating potential fluctuations in edge plasmas are illustrated in figure 2, showing the spectra of cross-power, coherence and toroidal mode number between two $\tilde{\phi}_\mathrm{f}$s on probe arrays A and B at $r - a = -1.0\,\mathrm{cm}$, respectively. It should be noted that the cross-power spectrum between two $\tilde{\phi}_\mathrm{f}$s with a large toroidal separation could highlight the spectral structures of long-range coherent modes with less disturbance of ambient turbulence. The spectra are averaged over 300 realizations with a frequency resolution of 1 kHz, which is the default resolution in the following figures unless with additional description. Two coherent modes peaked at frequencies of 12 and 21 kHz appear in the cross-power spectra, demonstrating strong correlation over a distance of 256 cm toroidally, as shown in figures 2(*a*) and (*b*). The phase shifts of the two coherent modes appear to be almost zero and the corresponding mode numbers are much smaller than one, as illustrated in figure 2(*c*), suggesting that both modes are toroidally symmetric. A comparison of the auto-power spectra between the Mirnov coil data and the floating potential is also shown in figure 3(*a*). It could be found that the MHD oscillation at 4 kHz has little influence on the potential fluctuations. A typical profile of T_e measured by the reciprocating probe array is given in figure 3(*b*), showing that the electron temperature at $r - a = -1.0\,\mathrm{cm}$ is about 50 eV.

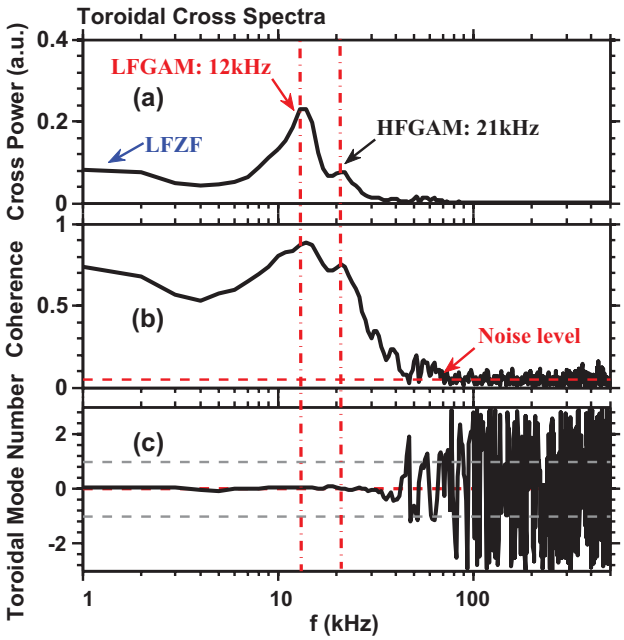

Figure 2. Spectra of (*a*) cross-power, (*b*) coherence and (*c*) toroidal mode number estimated from potential fluctuations on probe arrays A and B toroidally separated by 256 cm in shot 113901.

According to the measured electron temperature, the GAM frequency calculated from $f^{\rm th}_{\rm GAM} = \sqrt{(T_{\rm e} + 7T_{\rm i}/4)/m_{\rm i}}/\sqrt{2}\pi R_0$ [28] is 13 kHz with the assumption of $T_{\rm i} = T_{\rm e}$, which seems to access the mode peaking at 12 kHz, while the 21 kHz coherent mode may be another GAM generated inside and then propagated outwards. To distinguish the coexisting GAMs, the two modes at 12 kHz and 21 kHz would be called a low-frequency GAM (LFGAM) and a high-frequency GAM (HFGAM), respectively, in the following. Then their characteristics, especially the property of radial propagation, will be given first.

3.2. Identification and characteristics of KGAM

The radial propagation of the LFGAM and the HFGAM could be estimated when probe arrays A and B are placed with a radial separation of several millimetres. The phase shift measured by the two probe tips is composed of both radial and toroidal components, i.e. $\Delta\theta_{\rm AB}(f) = k_r(f)d_r + k_\phi(f)d_\phi$. Because the toroidal wavenumber k_ϕ for GAM is zero and its contribution to phase shift is negligible, $\Delta\theta_{\rm AB}$ can be used to estimate the radial wavenumber k_r for GAM.

The cross-power spectra between two $\tilde{\phi}_{\rm f}$s on probe arrays A and B, the amplitudes, central frequencies and radial wavenumbers of the LFGAM and the HFGAM at four radial positions inside the LCFS are shown in figure 4. The cross-power spectra at different radial positions in figure 4(*a*) illustrate the radial distributions of amplitude and central frequency of the LFGAM and the HFGAM. The GAM amplitude is calculated here from the integration of cross-power density spectra on the special frequency band determined by the central frequency and spectral width of the GAM. It could be seen from figure 4(*b*) that the amplitudes of the HFGAM keep growing in the radially inward direction, while the amplitudes of the LFGAM have a maximum value at $\Delta r \equiv r - a = -1.0$ cm. And although the amplitudes of the LFGAM are always larger than those of the HFGAM, the HFGAM decays less slowly than the LFGAM. From figure 4(*c*), it could be found that the central frequencies of both LFGAM and HFGAM remained almost constant in the range of measurement, with 1–2 kHz fluctuations. The eigenmode-type property have already been reported on JFT-2M, ASDEX-U, HL-2A and DIII-D [10, 11, 13, 15], as well as the simulations [29]. To seek the relationship between the LFGAM, the HFGAM and the continuum GAM, theoretic GAM frequencies $f^{\rm th}_{\rm GAM}$ are also plotted in figure 4(*c*), and it seems that the frequency of the LFGAM is consistent with the continuum GAM at $\Delta r \sim -0.8$ cm and the frequency of the HFGAM is possibly consistent with the continuum GAM at $\Delta r \sim -2$ cm.

The radial profiles of k_r for the LFGAM and the HFGAM are illustrated in figure 4(*d*). For the HFGAM, k_r remains positive in the whole measurement range, indicating that the HFGAM keeps propagating outwards, while for the LFGAM, k_r changes sign between $\Delta r = -0.5$ cm and $\Delta r = -1$ cm, probably at $\Delta r = -0.8$ cm, indicating that the LFGAM propagates in opposite directions on both sides of this position, which implies that $\Delta r \sim -0.8$ cm with $k_r \simeq 0$ may be the position where the LFGAM is generated. Similarly, it could also be deduced that the HFGAM is probably generated at $\Delta r \sim -2$ cm with $k_r \simeq 0$. Comparing with figure 4(*b*), it seems that the LFGAM and the HFGAM both have maximum amplitudes near the generation positions, suggesting that the mode amplitude peaks as excitation and decays as propagation. Then, going back to figure 4(*c*), it could be seen that the frequencies of the LFGAM and the HFGAM are just consistent with continuum GAM frequencies at $\Delta r \sim -0.8$ cm and $\Delta r \sim -2$ cm, which happen to be the positions where k_r is close to zero.

According to the KGAM theory, the fluid assumption is valid as the GAM remains as a long-wavelength structure, i.e. $k_r \simeq 0$, and the kinetic effect should be taken into account as the fluid approximation breaks down [19], explaining well why the measured frequencies are closest to the continuum GAM $f^{\rm th}_{\rm GAM}$ at positions with $k_r \simeq 0$. Moreover, it has been pointed out theoretically that different from the long-wavelength limit situation, the short-wavelength GAM itself is heavily damped by the high-order resonance [30], consistent with the radial relationship between amplitude and k_r of the LFGAM and the HFGAM. So it could be deduced that the LFGAM and the HFGAM are probably two KGAMs excited from the GAM continuous spectrum at the edge plasma, with radial wavenumbers close to zero at the excitation locations. Then the modes propagated both inwards and outwards, and during the propagation their amplitudes decreased with increasing absolute radial wavenumbers. The whole phenomenon is consistent with the mode conversion process from a continuum GAM to a KGAM predicted by the KGAM theory and simulations [18, 19, 31].

3.3. Nonlinear couplings between KGAMs

Bispectral analysis is used to investigate the nonlinear interaction between the LFGAM and the HFGAM, which is a powerful fluctuation analysis technique for detecting

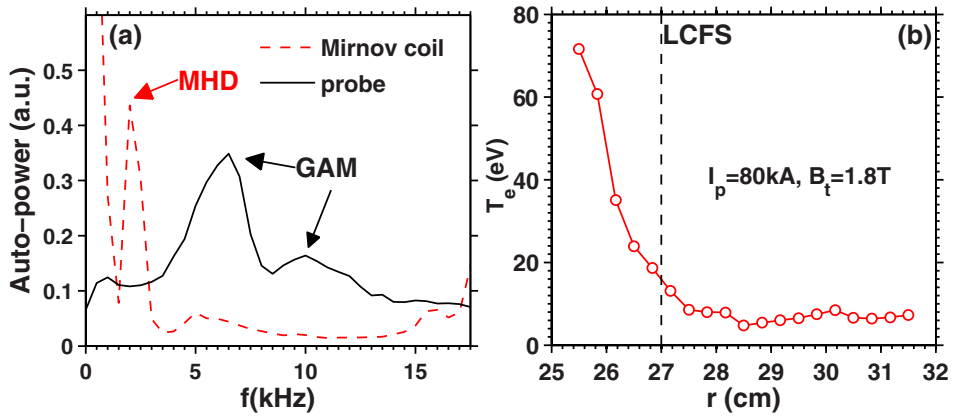

Figure 3. (*a*) Auto-power spectra of Mirnov coil data and floating potential data from probes. (*b*) Typical profile of T_e at the edge plasma measured by a reciprocating probe array under $I_p = 80\,\mathrm{kA}$, $B_t = 1.8\,\mathrm{T}$ and $n_e = 1.5 \times 10^{19}\,\mathrm{m}^{-3}$.

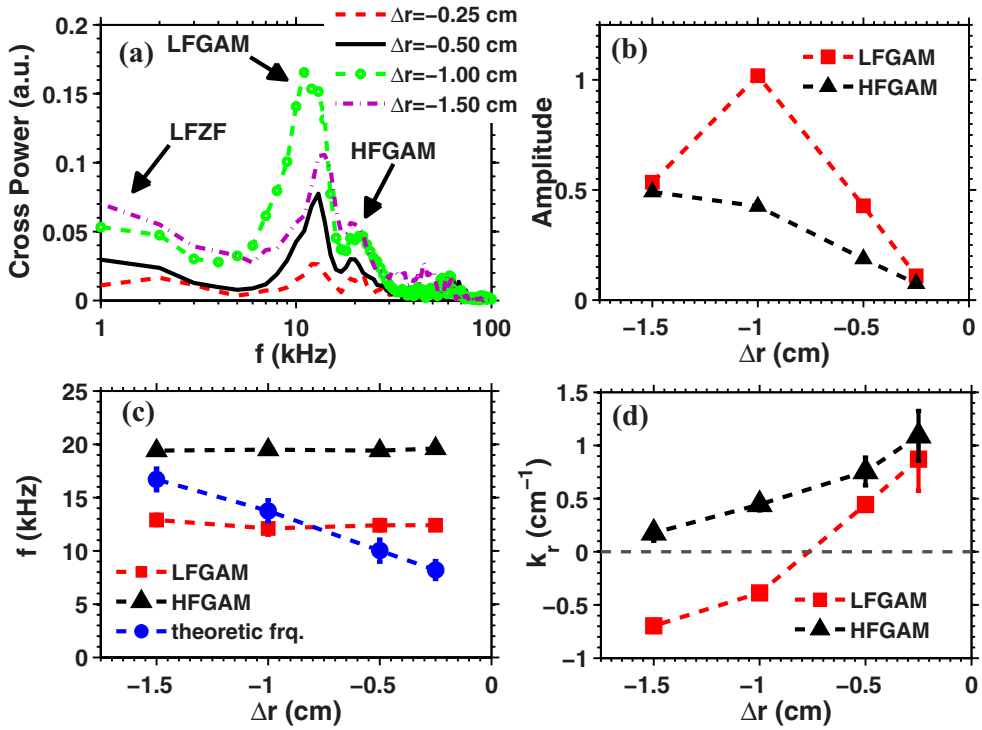

Figure 4. (*a*) Cross-power spectra between two toroidally separated floating potentials at four radial positions inside the LCFS; radial distributions of (*b*) the amplitudes, (*c*) the central frequencies and (*d*) the radial wavenumbers for the LFGAM and the HFGAM, and the profile of continuum GAM frequencies $f_{\mathrm{GAM}}^{\mathrm{th}} = \sqrt{(T_e + 7T_i/4)/m_i}/\sqrt{2}\pi R_0$ is also plotted for comparison. Data are from shots 113903, 113906, 113908 and 113909, respectively.

the strength of nonlinear three-wave interactions among the fluctuating quantities [32]. The squared auto-bicoherence $b^2(f_1, f_2)$ and the auto-biphase $\theta(f_1, f_2)$ are defined as

$$B(f_1, f_2) = \langle X(f_1)X(f_2)X^{\star}(f_3 = f_1 + f_2)\rangle \quad (1)$$

$$b^2(f_1, f_2) = \frac{|B(f_1, f_2)|^2}{\langle|X(f_1)X(f_2)|^2\rangle\langle|X(f_3)|^2\rangle} \quad (2)$$

$$\theta(f_1, f_2) = \tan^{-1}\frac{\mathrm{Im}[B(f_1, f_2)]}{\mathrm{Re}[B(f_1, f_2)]} \quad (3)$$

where $X(f)$ is the Fourier transform of the given time series, which is the floating potential fluctuation $\tilde{\phi}_f(t)$ here. Another commonly used quantity is the summed squared bicoherence $\Sigma b^2(f)$, which is defined as a sum of $b^2(f_1, f_2)$ for all f_1 and f_2 satisfying $f = f_1 + f_2$ and normalized by $N(f)$, the number of Fourier components for each f in the summation, i.e. $\Sigma b^2(f) = \Sigma_{f=f_1+f_2} b^2(f_1, f_2)/N(f)$, providing a degree of all the nonlinear interactions involving the frequency component f. Figure 5(*a*) shows the surface plot of $b^2(f_1, f_2)$ in the f_1–f_2 plane for the potential fluctuations at $\Delta r = -1\,\mathrm{cm}$. Because for auto-bicoherence f_1 and f_2 is interchangeable, only the area with $f_1 > 0$ and $f_1 \geqslant f_2$ is shown. It should be noticed that $B(f_1, f_2)$ has the same absolute values at $(f_1, f_2, f_1 + f_2)$, $(f_1 + f_2, -f_1, f_2)$ and $(f_1 + f_2, -f_2, f_1)$, causing some quasi-symmetry of auto-bicoherence $b^2(f_1, f_2)$, which could be seen from

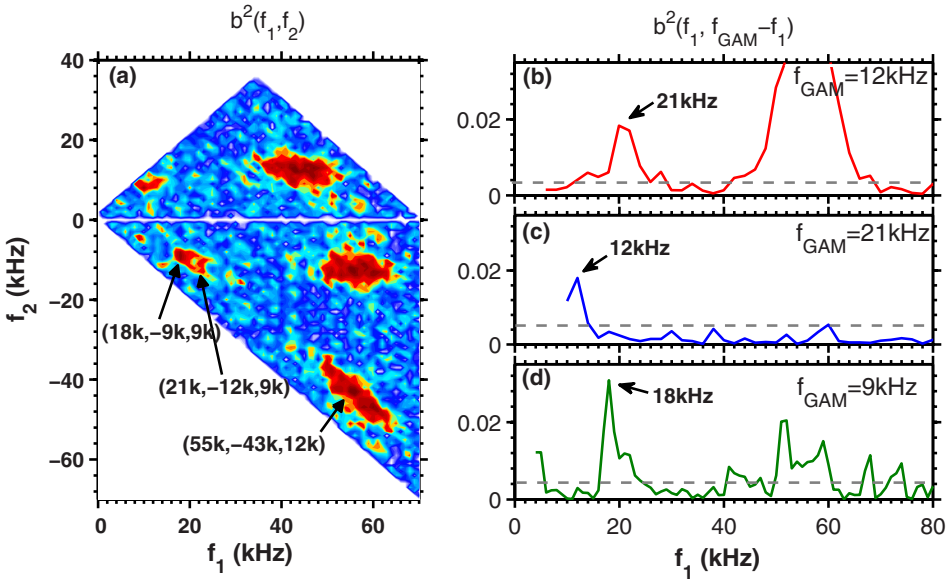

Figure 5. (*a*) Squared auto-bicoherence $b^2(f_1, f_2)$ of the floating potential fluctuations and auto-bicoherence $b^2(f_1, f_{\rm GAM} - f_1)$ as a function of f_1 for (*b*) $f_{\rm GAM} = 12$ kHz, (*c*) $f_{\rm GAM} = 21$ kHz and (*d*) $f_{\rm GAM} = 9$ kHz. The floating potential is from shot 113906.

figure 5(*a*). It could be found that the strongest interactions are concentrated at the three wave triads (9 kHz, 9 kHz, 18 kHz), (9 kHz, 12 kHz, 21 kHz) and (12 kHz, 43 kHz, 55 kHz), which could be seen more clearly from the bicoherences $b^2(f_1)$ for all frequencies obeying $f_1 + f_2 = 9$ kHz, $f_1 + f_2 = 12$ kHz and $f_1 + f_2 = 21$ kHz shown in figures 5(*b*)–(*d*).

Firstly, it could be found that the strongest interaction happens between the LFGAM and the quasi-coherence mode between 40 and 70 kHz, as indicated by the marker (55 kHz, −43 kHz, 12 kHz) in figure 5(*a*). The quasi-coherence mode is common in edge plasmas and has been reported both in TEXTOR and HL-2A [27, 33, 34]; however, its mode type and generation mechanism are still unknown. The strong nonlinear coupling implies that the quasi-coherence mode may play an important role in the self-organizing system of GAMs and ambient turbulence. Secondly, let us focus on the coupling of (9 kHz, 12 kHz, 21 kHz), which is definitely the interaction between the LFGAM and the HFGAM. According to the resonance conditions for three-wave interaction $f_1 \pm f_2 = f_3$ and $\vec{k}_1 \pm \vec{k}_2 = \vec{k}_3$, the component at 9 kHz should also be an azimuthally symmetric structure with $m = n = 0$. Going back to figure 2, the frequency component at $f = 9$ kHz is indeed toroidally symmetric and the only difference from the LFGAM/HFGAM is that its amplitude is smaller. Then, this is an obvious proof of the nonlinear interactions between the LFGAM and the HFGAM, which may play an important role during their saturation processes and has not yet been theoretically mentioned. Thirdly, based on the analyses above, the coupling of (9 kHz, 9 kHz, 18 kHz) should be the self-interaction of the 9 kHz component while the frequency component at $f = 18$ kHz is also a symmetric structure, which could also be verified through figure 2. Self-interaction of GAMs has been reported on the JFT-2M tokamak [20] and discussed in detail theoretically [21, 22].

It should be emphasized that the bispectral analyses above are only for the radial position at $\Delta r = -1$ cm, where the LFGAM reaches the maximum amplitude. In figure 6,

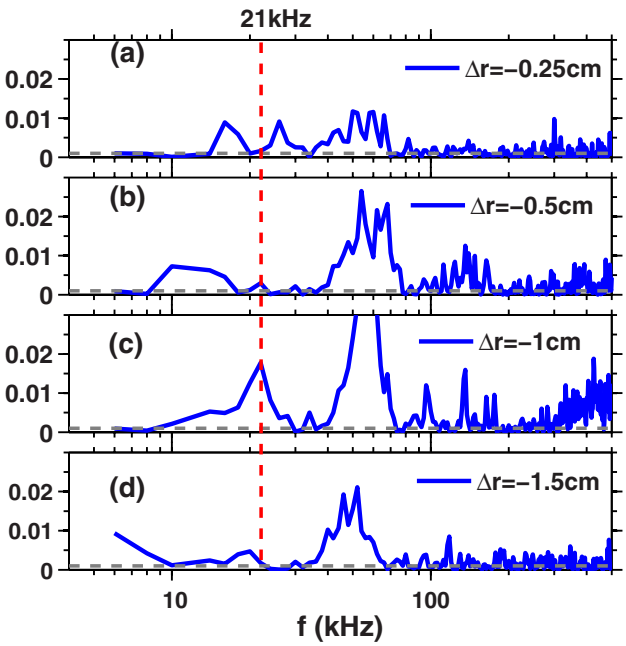

Figure 6. Squared auto-bicoherence $b^2(f_1, f_2)$ for $f_1 + f_2 = f_{\rm LFGAM}$ at different radial positions. Data used are the same as those in figure 4.

the auto-bicoherence $b^2(f_1, f_2)$ for all frequencies obeying $f_1 + f_2 = f_{\rm LFGAM}$ at four different radial positions is illustrated. It could be seen that the nonlinear coupling between the LFGAM and the HFGAM, i.e. the value of bicoherence $b^2(21\ {\rm kHz})$ is the strongest at $\Delta r = -1$ cm, and close to the noise level at the other three positions, as shown by the red dashed line. From figure 4, we know that the LFGAM has the maximum amplitude at $\Delta r = -1$ cm, suggesting that the nonlinear coupling between the LFGAM and the HFGAM occurs only when the amplitude of the LFGAM is sufficiently large. Furthermore, the coupling between the LFGAM and

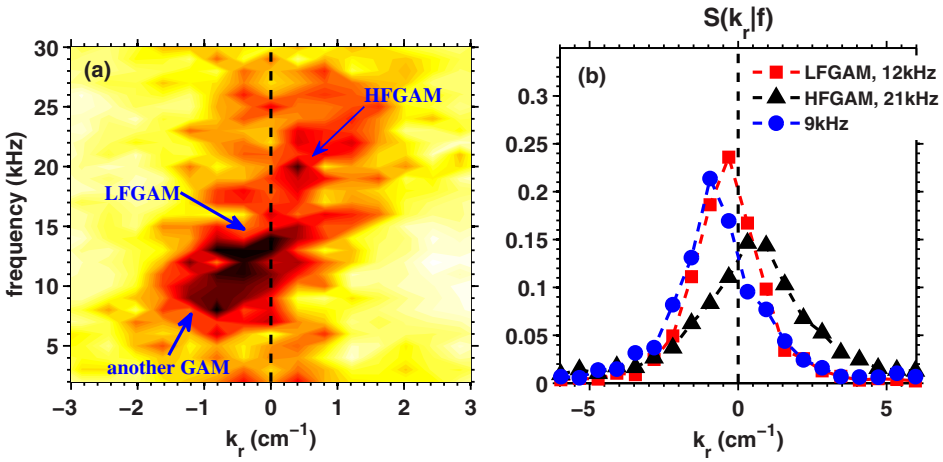

Figure 7. (*a*) Conditional wavenumber–frequency spectrum $S(k_r|f)$ below 30 kHz estimated from two potential fluctuations with a radial separation of 5 mm and toroidal separation of 256 cm. (*b*) $S(k_r|f)$ at $f = 9$ kHz, $f = f_{\mathrm{LFGAM}}$ and $f = f_{\mathrm{HFGAM}}$. The two floating potentials are from shot 113906.

the quasi-coherence mode at $f \approx 50$ kHz, and the coupling between the LFGAM and ambient turbulence beyond 200 kHz are both largest at $\Delta r = -1$ cm. These phenomena suggest that the interactions between the LFGAM and other modes (including both HFGAM and other ambient turbulence) are all closely related to the amplitude of the LFGAM, which has some similarities with the simulated result that the generation rate of the second harmonics is proportional to the intensity of the pump GAM [21].

Overall, besides the conventional coupling between the GAM and the high-frequency turbulence ($f > 200$ kHz), the bicoherence analyses here show three other types of nonlinear interactions: the coupling between the LFGAM and the HFGAM, the self-coupling of the GAM with the beat frequency between the LFGAM and the HFGAM, and the coupling between the LFGAM and the quasi-mode around 50 kHz. The intensities of these couplings all strongly depend on the amplitude of the LFGAM. To totally unravel the underlying physics during the saturation process of GAMs, these interactions should be paid more attention and more analyses are needed in the future.

3.4. Radial couplings between the LFGAM and the HFGAM

To further study the coupling between the LFGAM and the HFGAM, the local wavenumber–frequency spectrum $S(k_r, f)$ at $\Delta r = -1$ cm is estimated. $S(k_r, f)$ is calculated through the two-point cross-correlation technique [35], which has been widely used for characterizing plasma turbulence. This approach is based on the assumption that fluctuations can be described as a superposition of wave packets each being characterized by a stochastic relationship between wavenumber k_r and frequency f. Contour plots of conditional wavenumber–frequency spectrum $S(k_r|f) = S(k_r, f)/S(f)$ with $S(f) = \Sigma_{k_r} S(k_r, f)$ for $\tilde{\phi}_{\mathrm{f}}$s with a radial separation of $d = 5$ mm are shown in figure 7, as well as $S(k_r|f)$ at three given frequencies. From figure 7(*a*), it could be found that besides the two noticeable peaks of the LFGAM and the HFGAM, another peak concentrated around $f = 9$ kHz in the negative territory could also be observed. $S(k_r|f)$ at the LFGAM, the HFGAM and $f = 9$ kHz is plotted in figure 7(*b*), and the spectrally averaged radial wavenumber $\bar{k}_r$ and the wavenumber width σ_{k_r} could be estimated by

$$\bar{k}(f) = \int \mathrm{d}k\ S(k|f)\ k \tag{4}$$

$$\sigma_k^2(f) = \int \mathrm{d}k\ [k - \bar{k}(\omega)]^2 S(k|f). \tag{5}$$

For the LFGAM, $\bar{k}_r = -0.39\,\mathrm{cm}^{-1}$ and $\sigma_{k_r} = 1.51\,\mathrm{cm}^{-1}$, while for the HFGAM, $\bar{k}_r = 0.44\,\mathrm{cm}^{-1}$ and $\sigma_{k_r} = 2.25\,\mathrm{cm}^{-1}$. The averaged radial wavenumbers are consistent with the values calculated from the phase shift $\Delta\theta_{\mathrm{AB}}$, which are used to calculate the radial wavenumbers in figure 4(*d*). For $f = 9$ kHz, $\bar{k}_r = -0.71\,\mathrm{cm}^{-1}$, $\sigma_{k_r} = 1.70\,\mathrm{cm}^{-1}$. It is interesting to note that $\bar{k}_{r,9\,\mathrm{kHz}}$ is close to the wavenumber difference between the LFGAM and the HFGAM, $\bar{k}_{r,\mathrm{LFGAM}} - \bar{k}_{r,\mathrm{HFGAM}} = -0.83\,\mathrm{cm}^{-1}$, corroborating the nonlinear coupling between the LFGAM and the HFGAM.

3.5. Energy flow during the self-interaction of GAMs

When the plasma current is increased to $I_{\mathrm{p}} = 120$ kA with the magnetic field and the chord-averaged electron density nearly unchanged, multi-GAMs would appear. Figure 8 shows the spectra of cross-power, coherence and toroidal mode number between two $\tilde{\phi}_{\mathrm{f}}$s on probe arrays A and B at the same radial locations and several peaks could be observed in the frequency range between 6 and 40 kHz. Similar to the analyses of figure 2, these modes with high coherences and symmetric structures are essentially attributed to GAMs. Considering that the spectral width of a GAM is usually several kilohertz at the edge plasma [14, 23, 26, 27, 33], there should be several GAMs in such a frequency range larger than 30 kHz. Assuming the spectral shape for each GAM satisfies the Lorentzian distribution in the frequency domain, the cross-power spectrum between 6 and 40 kHz could be fitted by five summed Lorentzian functions, as illustrated in figure 8(*a*). The fitting result shows good consistency with the cross-power spectrum and the central frequencies of the five fitted functions are 12, 15, 18, 24 and 30 kHz. Through the bicoherence analysis, it could be found that the GAMs at 24 and 30 kHz are the second harmonics of the

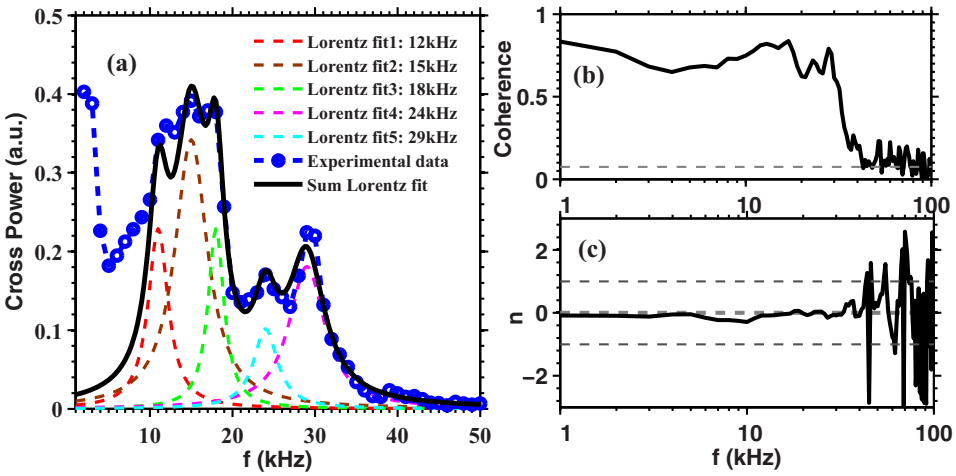

Figure 8. Spectra of (*a*) cross-power, (*b*) coherence and (*c*) cross-phase estimated from potential fluctuations of two different toroidal positions A and B (ϕ_A and ϕ_B) in shot 113170. Probes A and B were set at the same radial position.

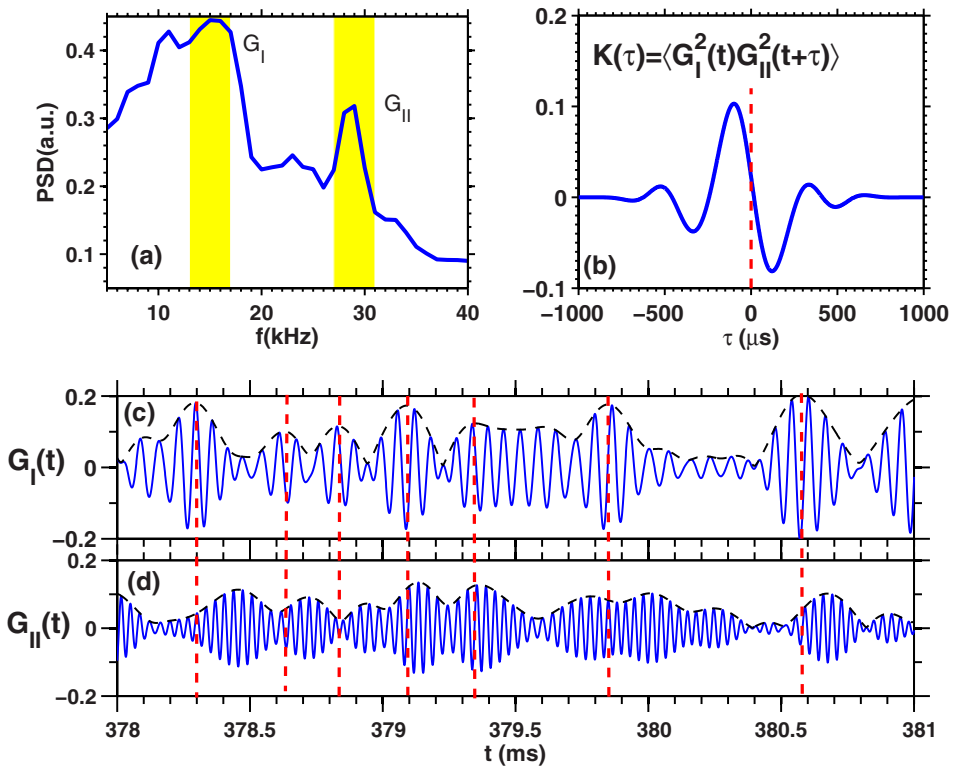

Figure 9. (*a*) Auto-power spectrum of $\tilde{\phi}_f$. G_I and G_{II} are the fundamental GAM and the second harmonic GAM filtered from 14–18 kHz and 27–31 kHz, respectively, (*b*) the CCF $K(\tau) = \langle G_I^2(t) G_{II}^2(t+\tau)\rangle$, and the temporal evolutions of $G_I(t)$ and $G_{II}(t)$ in 3 ms, with envelopes marked as black dashed curves.

GAMs at 12 and 15 kHz, again emphasizing the important role of the self-interaction of GAMs. This spectrum could be used to study the spectral energy transfer between the fundamental GAM and the second harmonic GAM.

To identify the energy flow direction between the fundamental GAM and the second harmonic GAM, the amplitude correlation technique [36, 37] is used on the GAMs at 15 and 30 kHz. By comparing the time delay between the envelopes of two time series $x_1(t)$ and $x_2(t)$, the cross-correlation function (CCF) $K(\tau) = \langle x_1^2(t) x_2^2(t+\tau)\rangle$ could estimate the energy flow direction between the two time series. The technique could be used to study the spectral energy transfer between different scales [38]. Shown in figure 9(*a*) is the power spectrum of the floating potential fluctuations, and the shaded spectra regions of 13–17 kHz and 27–31 kHz correspond to the fundamental GAM and second harmonic GAM, marked as G_I and G_{II}, respectively. The two time series are then squared and passed through a low-pass filter to obtain only the slowly varying amplitude information (with the dc components removed). Then the CCF $K(\tau)$ is computed, as shown in figure 9(*b*).

The CCF has a maximum at the negative time lag, which means that the amplitude of the harmonic GAM lags with respect to the fundamental GAM, which is further supported by

temporal evolutions of $G_{\mathrm{I}}(t)$ and $G_{\mathrm{II}}(t)$ shown in figures 9(*c*) and (*d*). It could be generally seen that the envelope of $G_{\mathrm{II}}(t)$ begins to increase after the envelope of $G_{\mathrm{I}}(t)$ reaches the local maximum. The interpretation of the time lag is that the second harmonic GAM receives energy from the fundamental GAM. In combination with the bicoherence analysis, it could be implied that the harmonic GAMs may be generated by the fundamental GAMs through self-nonlinear interactions.

4. Discussion

Compared with the single-peak GAM observed on the HT-7 tokamak in previous experiments [12], the coexisting multi-GAMs appeared when the walls were lithium coated with the discharge parameters changed slightly, so the wall condition must be the key factor to generate the multi-GAMs. It should be noted that the plasma responses to a lithium-coated wall have been measured on the NSTX tokamak [39, 40], showing that as a result of applying lithium coating on the graphite and plasma-facing components, the ion temperature at the edge plasma becomes higher while the ion density becomes lower, which means a decrease in the collision damping rate, and this would certainly benefit the generation and propagation of GAMs. This may be a possible mechanism to explain the multi-GAMs on HT-7. The radial profile of collisional damping of GAMs has been theoretically studied recently [41], indicating that the damping rate of GAMs is nonmonotonic as the collision rate increases, which may provide a possible candidate responsible for multi-GAMs.

As mentioned in the last section, the distributions of amplitude and radial wavenumber of the LFGAM and the HFGAM are qualitatively coincident with the process that KGAMs are converted from the GAM continuous spectrum. However, the KGAM theory indicates that KGAM will propagate at lower frequencies with respect to the GAM continuum frequency, i.e. towards the lower temperature or higher q region [19, 42], which seems inconsistent with the observed inward propagating LFGAM. In fact, based on figure 4(*b*), the decay length of the inward propagating LFGAM could be roughly estimated as 0.5 cm, much smaller than the averaged radial wavelength of the LFGAM $2\pi/\bar{k}_r \sim$ 12 cm, so the LFGAM is actually heavily damped as inward propagating, still in coincidence with the KGAM theory [42].

5. Conclusion

In conclusion, the propagating and coupling characteristics of coexisting multi-GAMs, especially dual GAMs at the edge of the HT-7 tokamak with lithium-coated walls are studied through Langmuir probe arrays. The mode structure and radial propagation of the coexisting dual GAMs are analysed in detail. Within the 2 cm measurement range inside the separatrix, it is found that the central frequencies of the LFGAM and the HFGAM remain nearly unchanged, and the radial positions with maximum amplitudes of the LFGAM/HFGAM happen to be where their k_rs are closest to zero and the continuum GAM frequency is closest to their central frequencies. According to the KGAM theory, $k_r \sim 0$ means a long-wavelength GAM, i.e. the theoretic fluid limit without kinetic effects. As k_r increases, the fluid approximation breaks down and the kinetic effects must be taken into account. Therefore, the LFGAM and the HFGAM could be explained as two kinetic eigenmodes generated from the continuum GAM, with their amplitudes peaked as excitation and decayed as propagation. Moreover, the bicoherence analyses indicate several types of nonlinear interactions in the low-frequency range ($f < 100$ kHz). In addition to the coupling between the HFGAM and the LFGAM, and the self-coupling of the other GAM with the beat frequency between the HFGAM and the LFGAM, the strongest coupling comes from the LFGAM and a quasi-mode at ~50 kHz. The coupling intensities all reach maximum near the exciting location of the LFGAM and these nonlinear interactions should be considered during the saturation process of GAMs in the edge plasmas. The coexisting multi-GAMs are also found and at least five peaks of GAMs could be observed, with two pairs of fundamental and second harmonic frequencies. The amplitude correlation technique shows that the spectral energy flows from the fundamental GAM into the second harmonic GAM, implying that the harmonic GAMs are generated from the fundamental GAMs.

Acknowledgments

The authors thank J.Q. Dong, Y.Z. Zhang, F. Zonca and Z. Gao for fruitful discussions, as well as the HT-7 Team for the support of these experiments. This work is supported by the Natural Science Foundation of China under Grant Nos 10875124, 10990210, 10990211, 10990212 and 10905057, the National Magnetic Confinement Fusion Energy Development Program of China under Grant Nos 2010GB107000 and 2011GB107001, the Knowledge Innovation Program of the Chinese Academy of Sciences under Grant No kjcx-yw-n28 and the Fundamental Research Funds for Central Universities under Grant Nos WK2030040019 and WK2030040026.

References

[1] Winsor N., Johnson J.L. and Dawson J.M. 1968 Geodesic acoustic waves in hydromagnetic systems *Phys. Fluids* **11** 2448–50
[2] Diamond P.H., Itoh S.-I., Itoh K. and Hahm T.S. 2005 Zonal flows in plasma—a review *Plasma Phys. Control. Fusion* **47** R35–161
[3] Fujisawa A. 2009 A review of zonal flow experiments *Nucl. Fusion* **49** 013001
[4] Conway G.D., Angioni C., Ryter F., Sauter P. and Vicente J. 2011 Mean and oscillating plasma flows and turbulence interactions across the L–H confinement transition *Phys. Rev. Lett.* **106** 065001
[5] Conway G.D., Scott B., Schirmer J., Reich M., Kendl A. and the ASDEX Upgrade Team 2005 Direct measurement of zonal flows and geodesic acoustic mode oscillations in ASDEX upgrade using doppler reflectometry *Plasma Phys. Control. Fusion* **47** 1165–85
[6] McKee R., Fonck R.J., Jakubowski M., Burrell K.H., Hallatschek K., Moyer R.A., Nevins W., Rudakov D.L. and Xu X. 2003 Observation and characterization of radially sheared zonal flows in DIII-D *Plasma Phys. Control. Fusion* **45** A477–85
[7] Melnikov A.V., Eliseev L.G., Gudozhnik A.V., Lysenko S.E., Mavrin V.A., Perfilov S.V., Zimeleva L.G., Ufimtsev M.V., Krupnik L.I. and Schoch P.M. 2005 Investigation of the plasma potential oscillations in the range of geodesic acoustic mode frequencies by heavy ion beam probing in tokamaks *Czech. J. Phys.* **55** 349–60

[8] Fujisawa A. *et al* 2004 Identification of zonal flows in a toroidal plasma *Phys. Rev. Lett.* **93** 165002

[9] Krämer-Flecken A., Soldatov S., Koslowski H.R., Zimmermann O. and the TEXTOR Team 2006 Properties of geodesic acoustic modes and the relation to density fluctuations *Phys. Rev. Lett.* **97** 045006

[10] Ido T. *et al* and the JFT-2M Group 2006 Geodesic acoustic-mode in JFT-2M tokamak plasmas *Plasma Phys. Control. Fusion* **48** S41

[11] Zhao K.J. *et al* 2010 Turbulence and zonal flows in edge plasmas of the HL-2A tokamak *Plasma Phys. Control. Fusion* **52** 124008

[12] Liu A.D., Lan T., Yu C.X., Zhang W., Zhao H.L., Kong D.F., Chang J.F. and Wan B.N. 2010 Spectral characteristics of zonal flows in the edge plasmas of the HT-7 tokamak *Plasma Phys. Control. Fusion* **52** 085004

[13] Conway G.D., Troster C., Scott B., Hallatschek K. and the ASDEX Upgrade Team 2008 Frequency scaling and localization of geodesic acoustic modes in asdex upgrade *Plasma Phys. Control. Fusion* **50** 055009

[14] Melnikov A.V. *et al* 2006 Investigation of geodesic acoustic mode oscillations in the T-10 tokamak *Plasma Phys. Control. Fusion* **48** S87–110

[15] Hillesheim J.C., Peebles W.A., Carter T.A., Schmitz L. and Rhodes T.L. 2012 Experimental investigation of geodesic acoustic mode spatial structure, intermittency, and interaction with turbulence in the DIII-D tokamak *Phys. Plasmas* **19** 022301

[16] Gao Z., Itoh K., Sanuki H. and Dong J.Q. 2006 Multiple eigenmodes of geodesic acoustic mode in collisionless plasmas *Phys. Plasmas* **13** 100702

[17] Itoh S.-I., Itoh K., Sasaki M., Fujisawa A., Ido T. and Nagashima Y. 2007 Geodesic acoustic mode spectroscopy *Plasma Phys. Control. Fusion* **49** L7

[18] Xu X.Q., Xiong Z., Gao Z., Nevins W.M. and McKee G.R. 2008 Tempest simulations of collisionless damping of the geodesic-acoustic mode in edge-plasma pedestals *Phys. Rev. Lett.* **100** 215001

[19] Zonca F. and Chen L. 2008 Radial structures and nonlinear excitation of geodesic acoustic modes *Europhys. Lett.* **83** 35001

[20] Nagashima Y. *et al* and the JFT-2M Group 2007 In search of zonal flows by using direct density fluctuation measurements *Plasma Phys. Control. Fusion* **49** 1611

[21] Zhang H.S., Qiu Z., Chen L. and Lin Z. 2009 The importance of parallel nonlinearity in the self-interaction of geodesic acoustic mode *Nucl. Fusion* **49** 125009

[22] Sasaki M., Itoh K., Nagashima Y., Ejiri A. and Takase Y. 2009 Nonlinear self-interaction of geodesic acoustic modes in toroidal plasmas *Phys. Plasmas* **16** 022306

[23] Zhao K.J. *et al* 2006 Toroidal symmetry of the geodesic acoustic mode zonal flow in a tokamak plasma *Phys. Rev. Lett.* **96** 255004

[24] Lan T. *et al* 2008 Spectral characteristics of geodesic acoustic mode in the HL-2A tokamak *Plasma Phys. Control. Fusion* **50** 045002

[25] Liu A.D. *et al* 2009 Characterizations of low-frequency zonal flow in the edge plasma of the HL-2A tokamak *Phys. Rev. Lett.* **103** 095002

[26] Nagashima Y. *et al* and the JFT-2M Group 2006 Observation of coherent bicoherence and biphase in potential fluctuations around geodesic acoustic mode frequency on JFT-2M *Plasma Phys. Control. Fusion* **48** A377

[27] Xu Y. *et al* and the TEXTOR Team 2011 Observation of geodesic acoustic modes (GAMs) and their radial propagation at the edge of the textor tokamak *Plasma Phys. Control. Fusion* **53** 095015

[28] Watari T., Hamada Y., Fujisawa A., Toi K. and Itoh K. 2005 Extension of geodesic acoustic mode theory to helical systems *Phys. Plasmas* **12** 062304

[29] Xu X.Q. *et al* 2009 Dynamics of kinetic geodesic-acoustic modes and the radial electric field in tokamak neoclassical plasmas *Nucl. Fusion* **49** 065023

[30] Sugama H. and Watanabe T.-H. 2006 Collisionless damping of geodesic acoustic modes *J. Plasma Phys.* **72** 825–8

[31] Qiu Z., Zonca F. and Chen L. 2011 Kinetic theories of geodesic acoustic modes: radial structure, linear excitation by energetic particles and nonlinear saturation *Plasma Sci. Technol.* **13** 257

[32] Kim Y.C. and Powers E.J. 1979 Digital bispectral analysis and its applications to nonlinear wave interactions *IEEE Trans. on Plasma Sci.* **7** 120 –31

[33] Lan T. *et al* 2008 Spectral features of the geodesic acoustic mode and its interaction with turbulence in a tokamak plasma *Phys. Plasmas* **15** 056105

[34] Zhao K.J. *et al* 2009 Two distinct regimes of turbulence in HL-2A tokamak plasmas *Nucl. Fusion* **49** 085027

[35] Beall J.M., Kim Y.C. and Powers E.J. 1982 Estimation of wavenumber and frequency spectra using fixed probe pairs *J. Appl. Phys.* **53** 3933–40

[36] Crossley F.J., Uddholm P., Duncan P., Khalid M. and Rusbridge M.G. 1992 Experimental study of drift-wave saturation in quadrupole geometry *Plasma Phys. Control. Fusion* **34** 235

[37] Duncan P.J. and Rusbridge M.G. 1993 The 'amplitude correlation' method for the study of nonlinear interactions of plasma waves *Plasma Phys. Control. Fusion* **35** 825

[38] Xia H. and Shats M.G. 2003 Inverse energy cascade correlated with turbulent-structure generation in toroidal plasma *Phys. Rev. Lett.* **91** 155001

[39] Bell M.G. *et al* and the NSTX Research Team 2009 Plasma response to lithium-coated plasma-facing components in the National Spherical Torus Experiment *Plasma Phys. Control. Fusion* **51** 124054

[40] Canik J.M. *et al* 2011 Edge transport and turbulence reduction with lithium coated plasma facing components in the National Spherical Torus Experiment *Phys. Plasmas* **18** 056118

[41] Gao Z. 2013 Collisional damping of the geodesic acoustic mode *Phys. Plasmas* **20** 032501

[42] Qiu Z., Chen L. and Zonca F. 2009 Collisionless damping of short wavelength geodesic acoustic modes *Plasma Phys. Control. Fusion* **51** 012001